Preamplifier Development for Superconducting Tunnel Junction Array X-ray Detector Electronics

W. K. Warburton, J. Harris, M. Carpenter, L. Fabris, and S. Friedrich

***Abstract*–We have developed a very low noise preamplifier that meets the low-cost, high-density requirements for use with superconducting tunnel junction (STJ) arrays. The design allows the STJs' bias points to be digitally set at the μV level. We then trace out noise versus bias curves under computer control and, by showing the correlation between this noise and detector energy resolution, establish the ability to automatically select optimum STJ operating points. Working with a 75 μm x 75 μm STJ with a Ta x-ray absorber, we achieved better than 7 eV FWHM at the 525 eV O-K line with about 2 eV coming from the preamplifier.**

I. Introduction

Superconducting tunnel junctions (STJs) can detect soft x-rays from 100 to 2000 eV with energy resolutions of 5 to 20 eV and count rates of 10 kcps or more [1-4]. Their use is complicated by Fiske mode resonances in their I-V curves, which are GHz cavity oscillation modes excited by the AC Josephson effect that degrade energy resolution by decreasing the detector's dynamic resistance if one coincides with the selected operating point. The separation between modes decreases with increasing pixel size, reaching 10 to 20 μV for STJs of about 200 x 200 μm, which precludes the use of larger sizes. Thus, STJs are typically used in arrays to increase their solid collection angle.

Used as x-ray detectors, STJs extend the powerful synchrotron radiation (SR) technique called XAS (x-ray absorption spectroscopy with fluorescence detection) into the 100 to 2000 eV regime, as shown by seminal work with a 36 element detector at the ALS [5-7]. This work made an excellent scientific case for going to even larger 100 to 1000 element arrays that would greatly increase sensitivity and enable the analysis of even more dilute specimens and solutions in the areas of materials analysis, biophysics, and environmental applications.

However, for widespread applicability in SR applications, these large arrays should be easy to operate by non-specialists and cost no more than present day HPGe hard x-ray detector arrays [8]. The first requirement requires that all setup and tuning operations, including finding an operating point that avoids Fiske modes, should be carried out automatically under computer control. The second, after subtracting detector and cryostat costs, means that the electronics must be delivered at about $250/channel, one tenth that of HPGe detectors, while preserving the STJs' superb energy resolution. This paper describes the development of a preamplifier for such a system.

II. Preamplifier Design

Our analysis of the STJ application produced the following preamplifier design requirements. Noise should be below 5 eV FWHM with an STJ dynamic resistance as low as 1000 Ω, implying an input referred noise of order 1 nV/√Hz. The input impedance should be < 10 Ω up to signal risetime frequencies of 200 kHz in order to avoid dynamical operating point shifts onto the Fiske mode resonances. The STJ's bias point must be adjustable over ± 1 mV under external computer control and held stably at the μV level. High packing density is also a requirement in array applications. Our target is 5 cm^2 of total board space. Finally, to reach a sales price of $250 per channel, its total electronics parts cost should be under $50. Of that, we allocated ~ $15 to the preamplifier, leaving $35 for the digital pulse processor. Both figures are aggressive.

Fig. 1 shows the class of topologies we investigated, which,

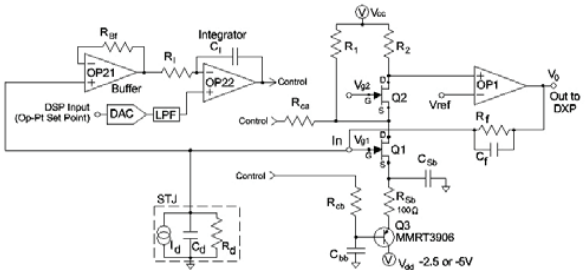

Fig. 1: Schematic of the investigated designs. Feedback can be provided through either input labeled "Control". When feedback is through R_{ca}, Q1's source is grounded (Designs W1 & W2) When feedback is through R_{cb}, then Q3 controls Q1's source voltage.

contrary to designs for semiconductor detectors, are transimpedance amplifiers with R_f of order 1 MΩ to satisfy our input impedance requirement. The control loop used to hold the bias point follows Friedrich's earlier design [9], with the addition of a serial DAC and low pass filter to remotely control the loop's set point. The amplifier follows the work of Fabris *et al*. [10] with a cascode input to an operational amplifier. The bias point could be stabilized either by connecting the feedback loop (Op Amps OP21 & OP22) to the drain of Q1 (via R_{ca}) or to its source (via R_{cb}). We tried the

Manuscript received November 13, 2010. This work was supported in part by the U.S. Department of Energy under Grant No. SC0002256.

W. K. Warburton is with XIA LLC, Hayward, CA 94544 USA (telephone: 510-401-5760, e-mail: bill@xia.com).

J. Harris is with XIA LLC, Hayward, CA 94544 USA (telephone: 510-401-5760, e-mail: jack@xia.com).

M. Carpenter is with Lawrence Berkeley National Laboratory, Berkeley, CA 94720 USA (telephone: 510-495-2889, e-mail: mhcarpenter1@lbl.gov) and also at Lawrence Livermore National Laboratory, Livermore, CA 94550.

L. Fabris is with Oak Ridge National Laboratory, Oak Ridge TN 37831 (telephone 865-576-2474, e-mail: fabrisl@ornl.gov).

S. Friedrich is with Lawrence Livermore National Laboratory, Livermore, CA 94550 (telephone 925-423-1527, e-mail: friedrich1@llnl.gov).

source stabilized mode both with Q3 and by directly tying Rcb to Q1's source. Because V_{g1} is the STJ's bias voltage and < 1 mV, its gate runs close to 0 V as well. Q1's V_{ds} is then set by $V_{g2}–V_{gs}$ of Q2. The current through Q1 is $(V_{cc}–V_{s2})/R_1 + (V_{cc}–V_{ref})/R_2$. The open loop gain is $g_{m1} R_2 A_1$, where A_1 is

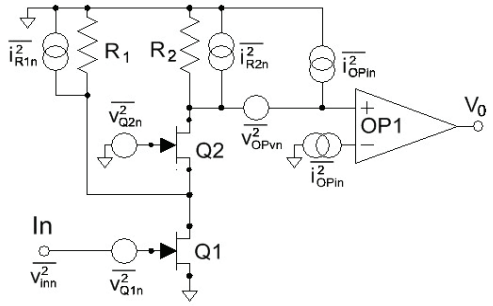

Fig. 2: Noise model of the preamplifier's inner loop

the gain of OP1. Since a 1 keV x-ray in the STJ generates about a 100 nA current pulse, using a 1 MΩ R_f results in 0.1 V output pulses.

Our noise analysis follows Fabris *et al*. [10] as shown in Fig. 2. The input referred voltage noise is found by converting the various noise terms into noise currents flowing through Q1 and then dividing by its transconductance g_{m1} to convert into noise voltages at its input. The resultant six terms are shown in (1) below. Because g_{m1} for our preferred BF862 input FET is about 40 mS, and it appears as g_{m1}^2 in all of the terms but the first, Q1 will usually be the major noise source. From the BF862's specified 0.8 nV/Hz^{½}, its effective value of

$$\overline{v_{inn}^2} = \frac{4kT\Gamma}{g_{m1}} + \frac{4kT\Gamma}{g_{m2}g_{m1}^2 r_{ds1}^2} + \frac{4kT}{R_1 g_{m1}^2} + \frac{4kT}{R_2 g_{m1}^2} + \frac{\overline{i_{OPin}^2}}{g_{m1}^2} + \frac{\overline{v_{OPvn}^2}}{g_{m1}^2 R_2^2} \quad . \quad (1)$$

Γ is 1.6. From Eqn. 2, we then calculate the output referred noise, which allows the noise terms to be scaled in eV by comparing their amplitudes to that of an x-ray pulse of known energy. Two terms are added to the inner loop amplifier noise: the feedback resistor's current noise $i_{Rfn} = \sqrt{(4kT/R_f)}$ and the STJ's quiescent tunneling current noise $i_{din} = \sqrt{(2eI)}$.

$$\overline{V_{0nn}^2} = \left[\frac{A Z_d}{Z_f + (A+1) Z_d}\right]^2 \left[\left(\frac{Z_d + Z_f}{Z_d}\right)^2 \overline{v_{inn}^2} + Z_f^2 \overline{i_{din}^2} + Z_f^2 \overline{i_{Rfn}^2}\right] \quad , \quad (2)$$

where A is the open loop gain and Z_f and Z_d are the feedback and detector impedances, respectively. Here $(Z_d + Z_f)/Z_d$ is the circuit's voltage noise gain and the leading bracketed term corrects for the amplifier's finite open loop gain.

The detector current noise term in Eqn. 2 also tells us the output voltage from an x-ray generated current pulse. Since STJs produce peak signals of ~100 nA/keV, the voltage output for R_f = 1 MΩ is about 0.1 mV/eV. We can then scale by this value to convert noise voltages into eV equivalents. Table I shows calculated noise values from the preamplifier's various components assuming reasonable part values, setting R_d to 1 kΩ and the effective bandwidth to 50 kHz (10 μs peaking time), and neglecting the impedances' reactive components. The results are shown both in μV and in eV FWHM by comparison to the 0.1 mV output pulse from a 1 eV photon absorbed in the STJ. While these values will

TABLE I. ESTIMATED NOISE VALUES (50 KHZ BANDWIDTH)

Part	Noise Term	Value	Component Values	$\sigma V_{n,rms}$ (μV)	FWHM (eV)
R_f	i_{Rfn}	$\sqrt{(4kT/R_f)}$	300K, $10^6\Omega$	29	0.7
STJ	i_{din}	$\sqrt{(2q\ I_d)}$	100 nA	40	0.9
Q1	v_{inn} term	$\sqrt{(4kT\ \Gamma/g_{m1})}$	300K, 40mS	179	4.3
Q2	”	$\sqrt{(4kT\ \Gamma/g_{m2})}$ / $g_{m1}\ r_{ds1}$	300K, 40mS; 40mS, $10^4\Omega$	0.5	0.1
R1	”	$\sqrt{(4kT/R_1)}/g_{m1}$	300K, $10^3\Omega$, 40mS	22	0.5
R2	”	$\sqrt{(4kT/R_2)}/g_{m1}$	300K, $10^3\Omega$, 40mS	22	0.5
OP1: i_n	”	i_{OPin}/g_{m1}	1.5pA/√Hz, 40mS	9	0.2
OP1: v_n	”	$v_{OPvn}/(g_{m1} R_2)$	1.7nV/√Hz, 40mS, $10^3\Omega$	9	0.2
TOTAL					4.5

change for different filters and components, they are very useful in guiding the design. As Table I shows, the major noise term is FET Q1, which, in quadrature, contributes >90% of the total noise for the low chosen value of R_d. The next largest term is the STJ's current noise, which will change with detector leakage current. The design is relatively insensitive to the input voltage noise of OP1 and to the values of the resistors R_1 and R_2, which means that R_1 can be adjusted to optimize the transconductance of Q1 and R2 to adjust the stage's gain. The results also emphasize the importance of finding operating points and/or devices with large R_d values since the major noise term scales as $1/Z_d$.

III. PREAMPLIFIER NOISE MEASUREMENTS

Evaluating the noise effects of small changes in preamplifier design is a non-trivial task at this level, both because of the low impedance of the intended detector and because access to operating STJ detectors is limited and expensive. Replacing the detector with the room temperature components of its equivalent circuit introduces a noise source – the resistor's thermal voltage noise – that dominates everything else. We therefore developed the following approach to accurately measure $\overline{v_{inn}^2}$. First, in (2) we replaced the STJ's current noise with a resistor's current noise and, assuming that the circuit's impedances are nominally resistive, recast (2) into (3),

$$\overline{V_{0nn}^2} = G_T^2 \left[(1+\frac{R_f}{R_d})^2 \overline{v_{inn}^2} + R_f^2 4k\frac{T_d}{R_d} + 4kT_f R_f + C\right] \quad (3)$$

where there are only three variables: the overall gain G_T^2, the input noise $\overline{v_{inn}^2}$ and an excess noise term added to account for pickup from environmental noise sources.

To measure a preamplifier's value of v_{inn}, its input referred noise, we applied a pulser to the dummy detector, input a pulse scaled to 1 keV in amplitude, and then measured the circuit's resolution using an XIA μDXP spectrometer. We made this measurement for 12 R_d values equally spaced in $1/R_d$ between 1/1000 and 1/20,000, plus the value $1/R_d = 0$, repeating at both room temperature (295 K) and liquid nitrogen temperature (77 K), and then made a fit to both temperature sets of data using (3) with only the 3 adjustable parameters G_T^2, $\overline{v_{inn}^2}$ and C.

Fig. 3 shows data taken on the optimized preamplifier W2 and fit using (3). As may be seen, there is extremely good

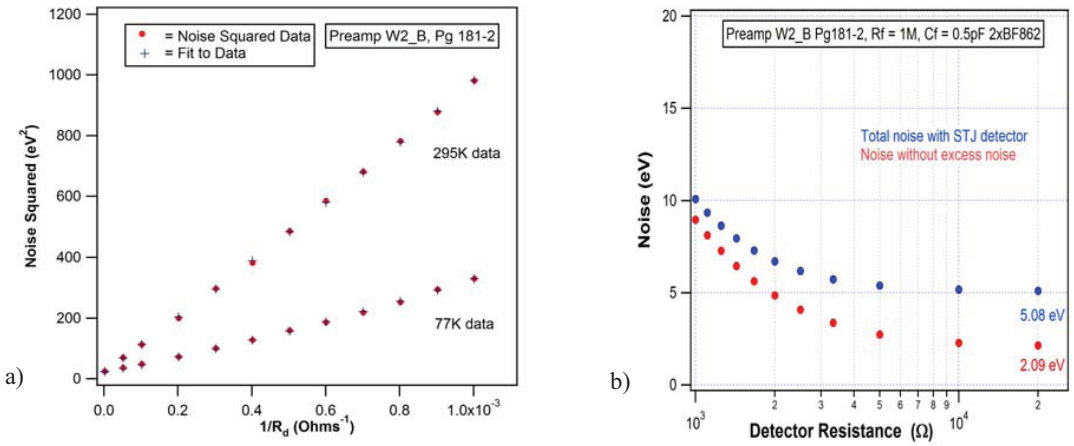

Fig. 3: Preamp W2: a) Fit to noise measurements versus $1/R_d$; b) Projected STJ noise versus STJ dynamic resistance

agreement between the data and the fitting function. v_{inn} is essentially extracted as the curvature in the data and, by using a specially designed cryostat that kept the "detector" resistors carefully shielded, we could measure v_{inn} at the 1% level. With this precision we could then reliably investigate the contributions to attainable resolution from sources such as power supply noise, g_{m1}, and feedback circuit noise.

IV. Selected Design – Performance and Cost

Using these methods, we fabricated and optimized four preamplifier designs and then compared them to the "LLNL" preamplifier currently used on the 36 element STJ array at the ALS [5-7, 9]. Our lowest noise variants for these designs are reported in Table II. Referring to Fig. 1, the designs are: "IV-1", an older design copying the LLNL design's use of a single 2SK147 FET as Q1, no cascode transistor Q2 or R1, and feedback through R_{ca}; "W1", with 1 BF862 FET as Q1, feedback through R_{ca}, and Q1's source grounded; "W2", the same as W1, but with two BF862 FETs in parallel for Q1; and "W5", with one BF862 Q1 and feedback through R_{cb}. The XIA W designs were primarily optimized by locating points where additional supply filtering helped and by varying the value of Q1's bias current.

The XIA IV-1 and LLNL preamplifiers, which share the same critical parts, produce comparable $\overline{v_{inn}^2}$ results, with the slight IV-1 improvement due primarily to heavier on-board power supply filtering. The new XIA W designs were all better than the IV-1 design, partially due to the addition of the cascode and partially because the BF862 appears to have better noise performance than the 2SK147. Of the W designs, W5 is noisier because any noise at Q1's source modulates V_{gs} and is directly injected into the circuit. W2 is slightly superior to W1, at the cost of an added Q1 transistor and its associated power draw, which may become significant in a large array design. Their comparison to the LLNL detector shows that both are viable designs for future development work.

Table II. "Best" preamplifier noise measurements

Parameter	LLNL	IV-1	W1	W2	W5
G_T^2 (10^{13})	10.989 ± 0.048	5.428 ± 0.026	5.389 ± 0.011	5.418 ± 0.016	5.438 ±0.015
$\overline{v_{inn}^2}$ (10^{-18} V²)	3.111 ± 0.073	2.778 ± 0.080	1.596 ± 0.042	1.389 ± 0.046	2.218 ± 0.046
C (10^{-13} V²)	4.42 ± 0.23	3.91 ± 0.26	5.68 ± 0.42	3.96 ± 0.16	3.24 ± 0.15
$\overline{v_{inn}}$ (nV/√Hz)	1.76 ± 0.02	1.67 ± 0.02	1.26 ± 0.02	1.18 ± 0.02	1.48 ± 0.02
Excess (eV)	6.97 ± 0.18	4.606 ± 0.15	5.53 ± 0.08	4.63 ± 0.09	4.20 ± 0.10

Using these fitting results, we can then project what energy resolution we would expect to obtain when the preamplifier is coupled to an STJ detector of a particular dynamic resistance R_d. Fig. 3b shows such a projection for preamplifier W2, both with and without the excess noise term. If R_d is large, we project that W2's noise contribution should be about 2 eV. As we report below, this is very close to the value found in a pulser measurement, validating our multi-resistor, two temperature measurement scheme.

Fig. 4 shows the complete design of our preferred W2 preamplifier, which uses a pair of BF862 FETs for Q11 and Q12 and a J310 for Q2. R_f is 1 MΩ, and C_f is 0.5 pF. In this design, Q11 and Q12 each draw I_{dss} = 14 mA, producing a parallel g_m of 84 mS. We note the heavy filtering of V_{cc} that

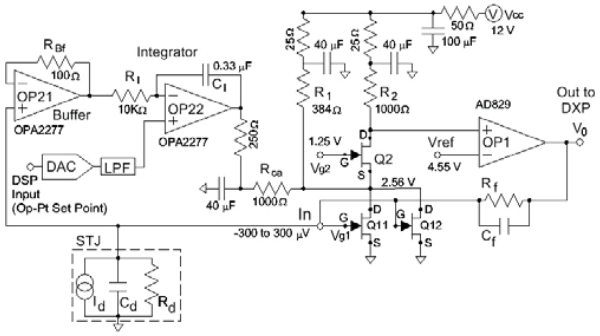

Fig. 4: Schematic diagram of preamplifier W2 design. Q11 and Q12 are BF862, Q2 is J310.

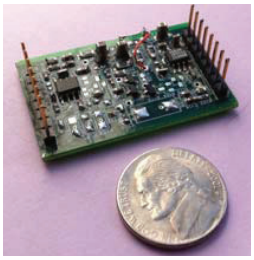

Fig. 5: The W2 preamplifier.

was needed to get the best performance. While we note that the LLNL preamplifier is traditionally operated from a battery supply to avoid this issue, there may be issues in trying to run 1000 preamplifiers from batteries in STJ detector array operation.

Fig. 5 shows the prototype W2 preamplifier on a 10 cm^2 PC board. The board is not densely populated, however, and our analysis shows that the final design should fit into less than 5 cm^2. This fully meets our space design constraint for high density array electronics, as will the W1 design, which has one fewer transistor.

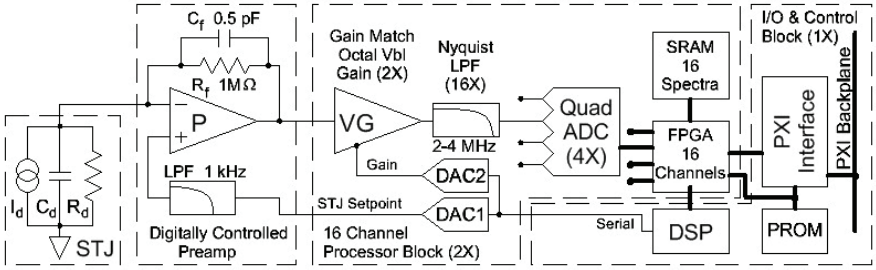

Fig. 6: Full system conceptual design for cost estimation.

The design's parts cost can now be calculated and comes to $13.20, which is comfortably below our $15 target. The most expensive single parts are the DAC, at about $2 and the OPA2277 dual Op Amp at $2.20. The most costly category is "passives" at $2.50, most of which is filtering capacitors. A future goal is to reduce this by finding ways of producing quieter V_{cc} supplies for the full, 32 channel board design.

In order to get a full channel cost estimate, we prepared a conceptual design of the full processing system as shown in Fig. 6. The design extends an in-house development board we had already built for another project and whose costs are well known. An octal variable gain amplifier matches the pre-amplifier output amplitudes, which are then Nyquist filtered and digitized by a quad or octal ADC before being digitally signal processed in a field programmable gate array (FPGA), which handles 16 channels (2/card) and saves spectra in local SRAM. A PXI interface is provided to the host computer. An on-board DSC is available for controlling various setup and calibration functions, particularly including adjusting the preamplifier's STJ bias voltages through their DACs. Using currently available parts and, without performing a detailed design that might simplify the design, we found an estimated parts cost of about $34/channel, leading to a full-system channel cost of $47, including the preamplifier, which nicely meets our design goal.

V. Noise Curve Measurements

To develop our noise curve measurement technique, we first made measurements with a conveniently available 200 µm x 200 µm STJ based on Nb-Al tunnel junctions made by Conductus, Inc. in the 1990's. Because it was not critical to this effort, we made no effort to optimize the STJ's energy resolution or reduce its current by improving its magnetic shielding. In these experiments we attached the STJ to a preamplifier and processed its output using an XIA µDXP digital x-ray spectrometer, typically with a 10 µs peaking time and 3 µs gap time. Taking advantage of our ability to set the STJ bias voltage under computer control, we devised a special program that stepped through a preset range of bias voltages and at each point collected 1000 baseline samples and then computed their mean and standard deviation from the mean. Since the µDXP is DC coupled, the baseline then measures preamplifier's DC offset, which equals the STJ's detector current times the feedback resistor R_f. Its variance is the electronic noise at the output of the preamplifier. Thus, by scanning, we can simultaneously plot out the detectors I-V curve and a "noise" curve versus bias voltage. We expect the I-V curve to display Fiske modes and for the noise curve

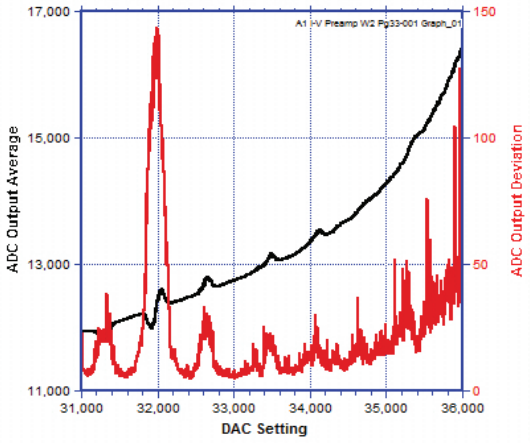

Fig. 7a: I-V and noise curves for a Nb STJ over a range of bias voltages.

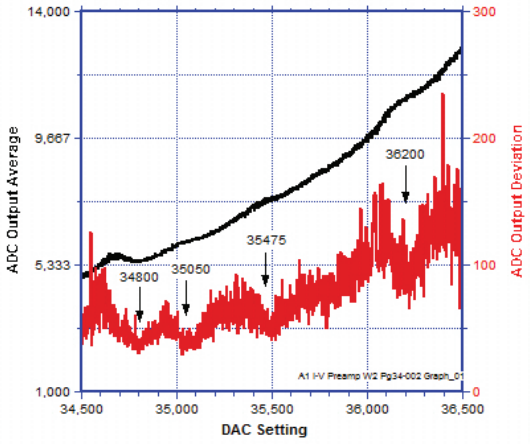

Fig. 7b: An expanded region of Fig. 7a, showing possible operating points.

to rise at these points, reflecting the impact of the Fiske modes on achievable energy resolution.

Figure 7a shows both I-V and noise curves for the 200 µm x 200 µm Nb device, with the I-V curve showing both the characteristic inflection at 0 bias, due to the DC Josephson current, and Fiske modes as the current increases. The noise curve behaves as expected, rising sharply at each Fiske mode. We note that the noise curve is a much more sensitive indicator, particularly at higher bias voltages where the Fiske modes become hard to observe.

Figure 7b is a scan with better statistics over a bias voltage region where we would like to locate an operating point. Even though the Fiske mode features in the I-V curve are relatively small here, the noise curve easily identifies four local noise minima as possible operating points.

We next made a series of resolution measurements in the vicinity of these operating points with the STJ detector exposed to radiation from the Fe_3O_4-coated anode of a Bremsstrahlung x-ray tube, which allowed us to see both O-K and Fe-L x-ray lines. Fig. 8 shows the resultant values of the energy resolution, FWHM, at the O-K line replotted onto Fig. 7b. It is clear that there is a good correspondence between minima in the noise curve and minima in resolution, allowing the noise curves, which can be collected in less than 1 minute to substitute for the resolution data (which took 2 hours to collect) in choosing a suitable bias point for detector operation. We believe that the small offset between the minima in the noise and energy resolution curves results from the preamplifier's finite open loop gain. During an x-ray current pulse the input has to move a few µV for the output to swing about 0.1 V.

Next, in preparation for measurements to evaluate our preamplifier's noise contribution to the energy resolution, we repeated these measurements using preamplifier W2 on a 67 µm x 67 µm STJ with a Ta x-ray absorber fabricated by Star Cryoelectronics. These measurements were carried out at at LLNL under conditions conducive to obtaining detector-limited performance, particularly, a cryostat that had good magnetic shielding, operation in a environment with a low EMI background, and the use of batteries to power the preamplifiers. Fig. 9 shows the I-V and noise curves that we

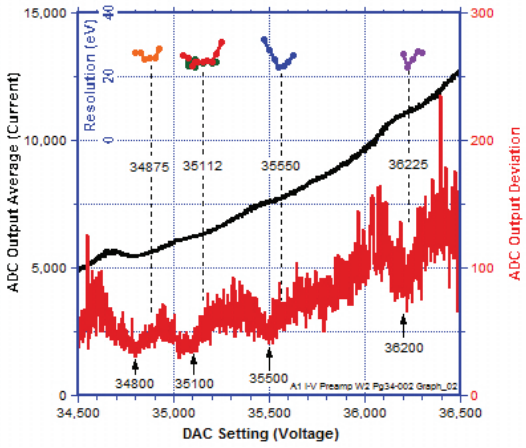

Fig. 8: Measured detector energy resolutions superimposed on Fig. 7b.

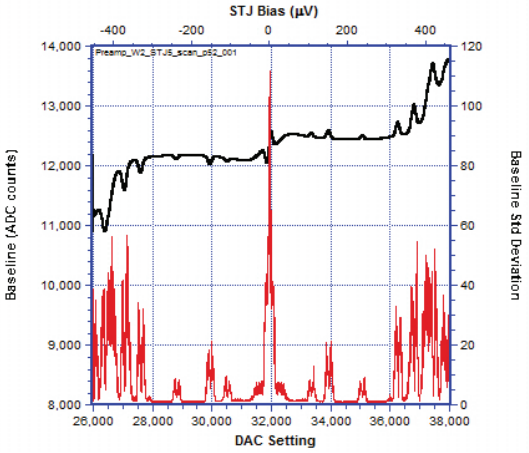

Fig. 9: I-V and noise curves for a Ta STJ over a range of bias voltages.

obtained under these conditions. We note that the I-V curve of this device shows much less leakage and that the noise curve is over an order of magnitude smaller between the first few Fiske modes than was the case in Fig. 7b. Also of interest is the bifurcation of the noise curve under each Fiske mode. This phenomenon originates in the detector's dynamical resistance, which goes to infinity (i.e. zero slope in the I-V curve) at the top of each Fiske mode and so reduces the preamplifier's noise, as may be seen from (2) and (3) with R_d set to infinity. As these splits are only 1-2 µV wide, their appearance testifies to the stability of the preamplifier's bias control feedback loop.

We next measured the detector's energy resolution at a series of about 50 closely spaced points covering the entire region where the noise floor was low, from 32,600 to 36,300 DAC steps (corresponding to 50 to 335 µV), with the results shown in Fig.10. We were consistently able to achieve better than 10 eV resolution except when crossing a Fiske mode, where it can double or triple, mirroring the structure of the noise curve with reasonable fidelity. This reinforces the observation that the noise curve (red) gives a much clearer view of when to expect energy degradation than the classic

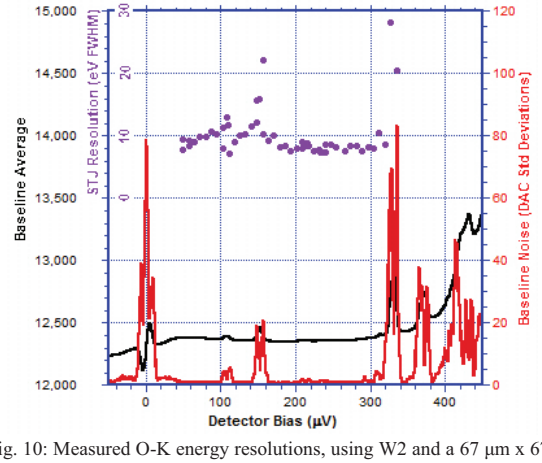

Fig. 10: Measured O-K energy resolutions, using W2 and a 67 µm x 67 µm Ta STJ, superimposed on a section of the noise curve shown in Fig. 9.

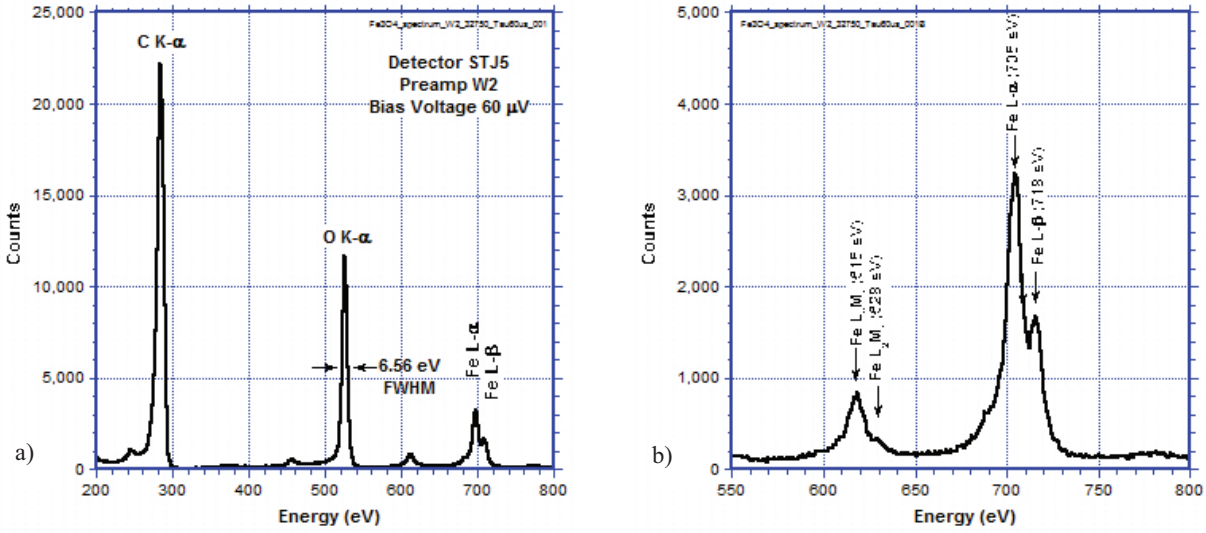

Fig. 11: a) Energy spectrum taken using preamplifier W2 attached to a 67 µm x 67 µm Ta STJ. b) Expanded Fe-L region of Fig. 11a.

I-V curve (black). We also note that the relative amplitudes of the Fiske modes changed slightly between Fig. 9 and Fig. 10, probably due to a slight change in magnetic field. Such changes emphasize the importance of being able to automatically verify STJ operating points when operating arrays with large numbers of elements.

VI. Energy Resolution measurements

Working from Fig. 10, we selected an operating point at 60 µV and collected a two hour spectrum from our Fe_3O_4 Bremsstrahlung x-ray source excited at 3 kV in order to get good counting statistics and also to provide a serious test of our preamplifier W2's long term stability. The full result is shown in Fig. 11a, with an energy resolution of 6.56 eV at the O-K line. Fig. 11b shows an enlargement of the region containing the Fe-L lines, whose structure is starting to resolve. In particular, the Fe-Lβ line at 717 eV is resolving on the shoulder of the Fe-Lα line at 704 eV that is twice as big. This combination of detector and preamplifier should therefore be excellent for synchrotron radiation research applications.

We also made measurements to directly compare our several preamplifier designs at the same STJ operating point. We began with a brief operating point search, using W2, as shown in Fig. 12, coupled with a few test resolution measurements. Three repeated measurements at 34350 DAC steps lead to essentially identical results, indicating that the selected point was stable. We also measured the preamplifier's noise at this same bias point using a pulser, obtaining a value of 2.5 eV, which is both twice as good as our design requirement of 5 eV and also very close to the number we estimated from our laboratory multi-resistor measurements.

We then collected resolution data for several of our preamplifiers at this fixed bias point, with the results shown in Fig. 13. Preamplifier W1 was broken at this time and could not be measured. As predicted from our noise analysis, Table II, W5 is worse than the other two new designs, which essentially deliver detector-limited energy resolutions, fully meeting out design goal. They also match the performance of

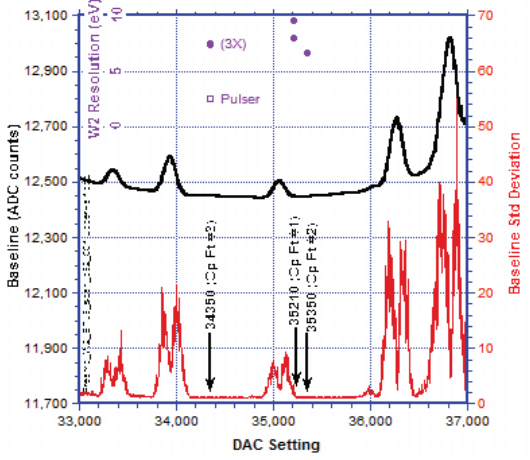

Fig. 12: I-V and noise curves for a Ta STJ over a range of bias voltages.

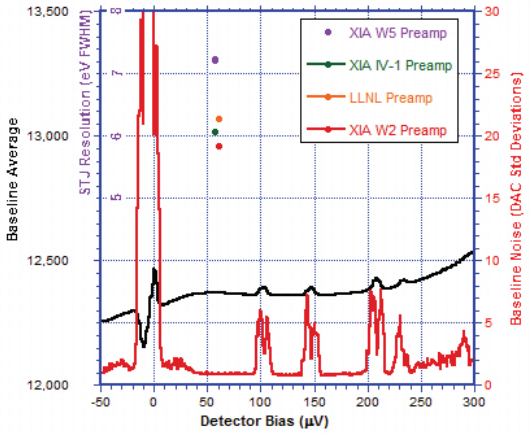

Fig. 13: Comparison for 4 preamplifier resolutions at 60 µV bias. Note the inset eV scale is only 5 – 8 eV.

the LLNL preamplifier, which has been a standard for many years. The difference between this result and that of Table II is that the LLNL preamplifier is more sensitive to power supply noise and here we were powering it from batteries, whereas in the laboratory measurements we used a filtered voltage regulator supply.

VII. Discussion and Conclusions

We designed and tested a preamplifier specifically intended to meet the requirements of instrumenting x-ray detector arrays with large numbers of STJ detectors. In particular, our design's 2.5 eV noise level will preserve the STJs' intrinsic energy resolution, as shown by our ability to achieve about 6 eV at the 525 eV O-K line with a 67 μm x 67 μm STJ with a Ta absorber. The parts cost for the design was only $13, which will allow complete digital spectroscopy electronics to be delivered commercially at about $250 per channel. The preamplifier has a feed-back stabilized bias set point whose operating voltage can be set and is stable at the μV level by a DAC, allowing full computer control. The entire design occupies about 5 cm^2, which meets high density packaging requirements. We will use the design to develop a 32 channel 3U card and test it with multiple elements simultaneously.

In developing the preamplifier, we devised a novel scheme to measure its input referred voltage noise with 1% precision by measuring its noise with a set of 12 dummy detector resistors at 298 K and 77 K and then doing a 3 parameter fit to extract v_{inn}, the input referred voltage noise. This capability was most useful, as it allowed us to track down and eliminate various non-intrinsic noise sources and to optimize the component values to obtain the best energy resolution without access to an STJ detector.

We also devised a procedure to use the computer controlled DAC in the preamplifier's bias control loop to trace out its noise as a function of the STJ's operating bias by stepping over a series of bias points and computing the standard deviation in our digital processor's baseline at each point. We showed a good correspondence between this noise curve and achievable x-ray energy resolution, so that, in large arrays, the 100 times faster noise measurement can be used to replace x-ray energy measurements to automate bias point selection procedures.

Acknowledgment

We particularly wish to thank Dr. Robin Cantor of Star Cryoelectronics for providing the high quality Ta-based STJ detectors used in this research, Dr. Peter Grudberg for adapting the μDXP code for making the noise measurements, and Ms. Ann Xiang for adding a special section to XIA's Omnivore code to read and display the STJ I-V curve and noise measurements.

References

[1] M. Frank *et al.*, "Energy Resolution and High Count Rate Performance of Superconducting Tunnel Junction X-ray Spectrometers", Rev. Sci. Instr. **69** (1998) 25-31.

[2] S. Bechstein *et al*., "Characterization of an Nb/Al/AlOx/Al/Nb superconducting tunnel junction detector with a very high spatial resolution in the soft X-ray range", Spectrochimica Acta **B59** (2004) 215-221.

[3] S. Friedrich, "Cryogenic X-ray detectors for synchrotron science", J. Synchrotron Radiation **13** (2006) 159-171.

[4] P. Verhoeve, "Photon Counting Low Temperature Detectors for Visible to Gamma Ray Astrophysics", J. Low Temp. Phys. **151** (2008) 675-683.

[5] T. Funk *et al.*, "Chemically Distinct Ni Sites in the A-Cluster in Subunit β of the Acetyl-CoA Decarbonylase/Synthase Complex", J. Am. Chem. Soc. **126** (2004) 89-95

[6] V. Lordi *et al.*, "Nearest-neighbor configuration in (GaIn)(NAs) probed by X-ray absorption spectroscopy", Phys. Rev. Lett **90** (2003) 145505.

[7] K. Ndung'u, S. Friedrich, A.R. Gonzales & A.R. Flegal, "Chromium oxidation by manganese (hydr)oxides in a California aquifer", Appl. Geochemistry **25** (2010) 377-381.

[8] H. Padmore, "Detector Needs and Plans for Soft XR/VUV/IR Science, "http://www.aps.anl.gov/ News/ Conferences/2005/Synchrotron _Radiation_Instrumentation /index.htm .

[9] S. Friedrich *et al*., "Single Photon Imaging Spectrometers Using Low Noise Current Preamplifiers with DC Voltage Bias", IEEE Trans. Appl. Superconductivity **7** (1997) 3383-3386.

[10] L. Fabris, N.W. Madden & H. Yaver, "A fast, compact solution for low noise charge preamplifiers", Nucl. Instr. & Methods in Phys. Res. **A424** (1999) 545-551.